

# Simulation and Experimental Investigation on Electrochemical Milling of TiB<sub>2</sub>/7050 Aluminum Matrix Composites

Yang Meng, Xiaoyun Hu, Hansong Li\*, Binsen He

Nanjing University of Aeronautics and Astronautics

\*E-mail: [hsli@nuaa.edu.cn](mailto:hsli@nuaa.edu.cn)

Received: 10 October 2022 / Accepted: 9 November 2022 / Published: 30 November 2022

TiB<sub>2</sub>/7050 aluminum matrix composite is a new particle-reinforced composite with excellent mechanical properties. However, owing to the presence of TiB<sub>2</sub>-reinforced particles in the material, its traditional machinability is inferior to that of the matrix aluminum alloy, and it becomes a typical difficult-to-machine material. Electrochemical milling (EC milling) is a non-traditional machining technology based on the principle of electrochemical anodic dissolution, and it is an effective way of machining difficult-to-machine metal materials. In this study, tool cathodes with concave arc surfaces that have different heights at the end of the tool are designed, and an electric field simulation and experimental investigation on the inner-jet EC milling of TiB<sub>2</sub>/7050 aluminum matrix composites are carried out. The electric field simulation results show that the higher the centre of the arc surface, the lower the current density. The arc surface tool allows for a more even distribution of charge through the machining area when the machining gap  $d = 0.3$  mm, and the electric charge distribution at the machining area under the tool with an arc centre height of 2 mm is the most uniform. An experimental investigation demonstrates that a tool with a concave arc surface at the end can improve the bottom surface flatness of the machined groove but at the cost of reducing the material removal rate (MRR). The bottom surface flatness of the groove machined by the tool with a 2-mm centre height on the curved surface was 13  $\mu\text{m}$  with a machining gap of  $d = 0.3$  mm. Compared with the flat-bottom tool, the flatness of the bottom surface was increased by 94.47%, but the corresponding MRR was reduced by 29.58%.

**Keywords:** Electrochemical milling, TiB<sub>2</sub>/7050 aluminum matrix composite, electric field simulation, bottom surface flatness, material removal rate

## 1. INTRODUCTION

TiB<sub>2</sub>/7050 aluminum matrix composites exhibit superior mechanical properties with higher strength, higher modulus of elasticity and hardness, improved fatigue resistance, better thermal stability, and higher wear resistance than the matrix 7050 aluminum alloy. [1–3]TiB<sub>2</sub>/7050 aluminum matrix composites are widely used in aerospace, transportation, and other industrial fields because of their

excellent overall mechanical properties. [4,5] However, owing to the existence of hard ceramic particles in the matrix, the tool experiences severe friction, high cutting forces, and high cutting temperatures during the machining process, which causes severe tool wear. Therefore, TiB<sub>2</sub>/7050 aluminum matrix composites with excellent physical properties are also considered difficult-to-machine materials. [6,7]

Electrochemical milling (EC milling) is a process that uses a geometric tool with a simple shape as the cathode and a workpiece as the anode to remove excess material from the workpiece like CNC milling, based on the principle of electrochemical anodic dissolution. EC milling has a high material removal rate (MRR), no wear of the tool cathode, and no residual stress, burr, heat-affected zones, etc. With this process, difficult-to-machine materials like TiB<sub>2</sub>/7050 aluminum matrix composites can be machined efficiently and flexibly, thereby reducing manufacturing costs. [8–10] Zhang et al. [11] conducted experiments on inner-jet EC milling of flat surfaces using large rectangular cathodes, it was found that an increase in the cathode feed rate could improve the uniformity of the machined surface. Ye et al. [12] designed inner-jet tubular tools with different wedge angles to change the electrolyte flow field, which in turn affected EC milling and demonstrated that a tubular electrode with a wedge angle of 40° yielded better machining accuracy and surface quality in the machining of deep and narrow grooves. He et al. [13] designed two cathodic tools for machining TiB<sub>2</sub>/7050 aluminum matrix composite workpieces using inner-jet EC milling. The research results showed that when the tool feed rate increased from 10 mm/min to 30 mm/min, the MRR increased from 94.4 mm<sup>3</sup>/min to 168.6 mm<sup>3</sup>/min, and the machined surface roughness (Ra) decreased from 5.787 μm to 3.329 μm, indicating that EC milling can improve the machining efficiency and surface finish by using an appropriate tool and machining conditions.

When machining TiB<sub>2</sub>/7050 aluminum matrix composites, after the grooves were machined by EC milling using the bottom of the cylindrical tool, the bottom surfaces of the machined grooves were uneven and tended to form an inwardly concave bottom surface. The bottom surfaces of the grooves were deep in the middle and shallow on the sides. Niu et al. [14] added a layer of insulating material to the bottom of a cylindrical tool when studying the embedded milling of difficult-to-machine alloys. The experiment revealed that the flatness of the bottom surface of the groove machined by the tool with the insulating layer was improved by approximately 58% compared with the tool without the insulating layer on the bottom surface. Li et al. [15] proposed a tool with an inwardly concave bottom surface that has a conical shape. The experiment revealed that the flatness of the bottom surface of the grooves machined by the tool with an inner tapered bottom surface was significantly improved compared to the grooves machined by the tool with a flat bottom.

The above research shows that for difficult-to-machine materials such as TiB<sub>2</sub>/7050 aluminum matrix composites, EC milling is a feasible processing method. However, the insulated bottom tool in the above study only had an improved effect on the bottom surface of the groove, and the effect of different taper of the tapered tool on the flatness of the groove bottom surface was not reflected. In response to the above problems, three kinds of tools with different heights of inner concave arc surface at the end were designed to study the relationship between charge distribution and flatness through electric field simulation. Subsequently, experiments were conducted to investigate the effects of different tools on the depth, MRR, and flatness of the bottom surface of the machined grooves under different machining gaps.

## 2. THEORETICAL ANALYSIS AND TOOL DESIGN

### 2.1 Theoretical analysis of groove concave bottom surface formation

Fig.1 shows a schematic diagram of the EC milling plane. The tool cathode machines the workpiece at a feed rate  $V_f$ , and the base radius of the tool is  $r$ . Points M and N are the two points in the machining groove, and the machining time for point M is  $2r/V_f$ , while that for point N is  $2r\cos\theta / V_f$ . According to Faraday's law, the volume of the anode material removed for some time can be expressed as [16,17]:

$$V = \int_0^t \eta \omega i dt \quad (1)$$

where  $\eta$  is the current efficiency,  $\omega$  is the volume electrochemical equivalent of the material, and  $i$  is the current density.

According to formula (1), it can be seen that the machining time of the middle point M of the groove is greater than that of point N on both sides. The volume of the material removed by electrolysis in the centre area is more significant than that on both sides, eventually causing the groove to have an uneven bottom surface.

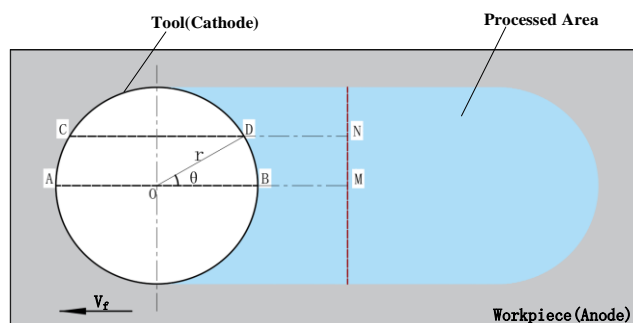
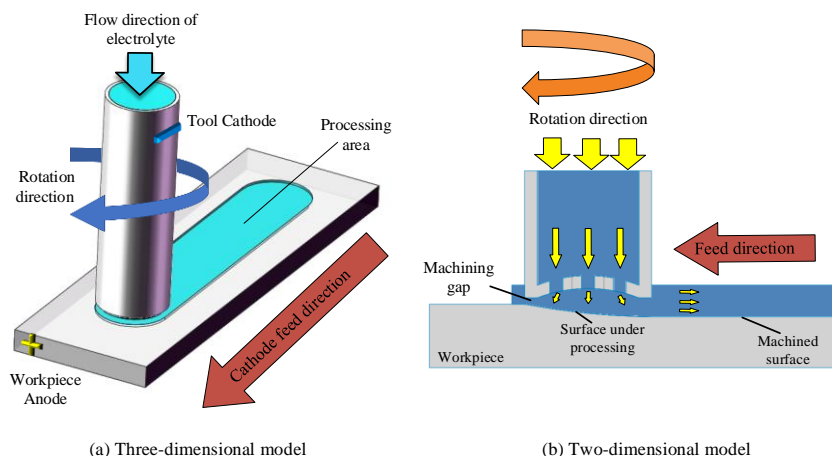


Figure 1. Schematic diagram of the EC milling process.

### 2.2 Machining principle and design of the inner-jet EC milling tool

Fig.2 shows the inner-jet EC milling method, where a tube electrode is a cathode and a high-speed electrolyte flows into the machining area through the inside of the tube electrode. During the machining process, the tubular tool rotated above the workpiece surface while machining in the feed direction. The electrolyte was injected into the machining gap through the through-hole at the bottom of the tool. The cathode (tool) and anode (workpiece) form a conductive circuit through the electrolyte flowing in the machining gap, and an electrochemical reaction occurred. The flowing electrolyte also removed the electrolysis products and the Joule heat formed by the electrochemical reaction of the anode of the workpiece. EC milling offers better processing flexibility than standard electrochemical machining (ECM). [18–21] In formula (1), the actual volume electrification equivalent  $\eta\omega$  and time  $t$  are constant in stable processing, and the magnitude of current density  $i$  can only be changed to balance the effect of the processing time. Therefore, the machining gap gradually decreased from the centre to the circumference with the introduction of a circular arc surface in the design of the tool end face, and the current density gradually increased, which led to a uniform amount of charge passing through the

machining area, thus providing a solution to improve the flatness of the bottom surface of the machined grooves.



**Figure 2.** Schematic diagram of inner-jet EC milling process.

Fig.3 shows a schematic diagram of two inner-jet EC milling tools: tool A and tool B. The outer wall of the tool is insulated to prevent the influence on the experiment; the outer and inner diameters of the tool are 20 mm and 18 mm, respectively, with a wall thickness of 1 mm and a diameter of 1.5 mm for the liquid outlet holes distributed on the machining surface at the bottom of the tool. The difference between tool A and tool B is that the bottom surface of tool A is a flat-bottom surface, while the bottom surface of tool B is a circular arc surface. The highest point of the circular arc surface is on the tool's centreline, the height from the tool bottom is  $h$ , and the chord length of the circular arc is 19 mm.

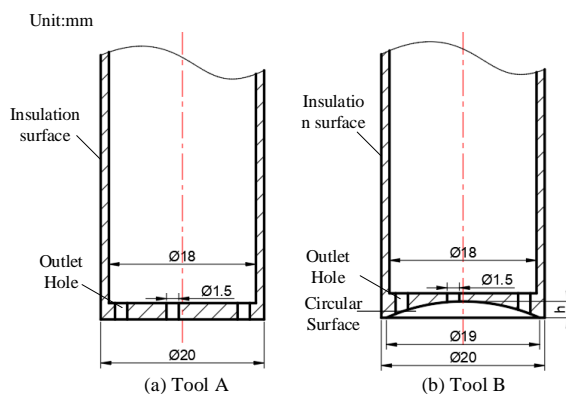


**Figure 3.** (a) Flat-bottom tool and (b) circular-bottom tool.

Fig.4 shows the tool designed with different curved surface heights to study the effect on the flatness of the groove bottom surface. Tools A, B, C, and D correspond to the centre height of the arc surface of 0 mm, 1 mm, 2 mm, and 3 mm, respectively, and tool A is the original control group. There is a layer of torus between the bottom arc surface of the tool and the cylindrical surface of the side wall to form a transition, the width of the torus is 0.5 mm, so the radius of the circle projected from the arc surface to the bottom is 9.5mm. The radii of the spheres on which the arc bottom surfaces of the tool cathodes B, C, and D are located can be determined from formula (2).

$$R^2 = (R - h)^2 + 9.5^2 \quad (2)$$

Where  $R$  is the radius of the spheres where the arc surface is located,  $h$  is the height of the arc surface, and  $9.5\text{mm}$  is the radius of the circle projected from the arc surface to the tool bottom. The resulting radii are  $45.63\text{ mm}$ ,  $23.56\text{ mm}$ , and  $16.54\text{ mm}$ , respectively.

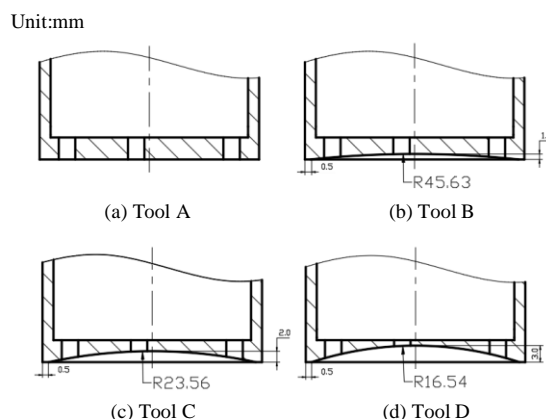


**Figure 4.** Schematic diagram of four sets of tool cathodes.

### 3. SIMULATION ANALYSIS

#### 3.1 Physics Model

Fig.5 simplifies the simulation model of the electric field where the cathode, anode, and machining gap are located. To more conveniently simulate the current density distribution during electrolytic machining and to simplify the calculation, the outlet holes at the bottom of the tool were ignored, that was, the bottom surface of the tool was considered smooth and complete. The following assumptions were made for the simulation conditions during the machining process.

- 1) The concentration gradient and temperature gradient of the electrolyte in the processing area  $\Omega$  are zero, and the conductivity is constant;
- 2) Both the cathode and anode surfaces are equipotential surfaces;
- 3) The reactions occurring during the process all follow Faraday's law.

Based on the above assumptions, the potential distribution within the processing region  $\Omega$  fits Laplace's equation [22,23]:

$$\nabla^2 \varphi = 0 \quad (3)$$

The boundary conditions satisfy the following conditions:

$$\varphi|_{\Gamma_{1,2,3}} = 0(\text{Cathode interface}) \quad (4)$$

$$\varphi|_{\Gamma_{6,7}} = U(\text{Anode interface}) \quad (5)$$

$$\frac{\partial \varphi}{\partial n}|_{\Gamma_{4,5}} = 0(\text{Insulation surface}) \quad (6)$$

Where  $\varphi$  is the potential,  $U$  is the anode potential, and  $n$  is a normal vector on the boundary surface.

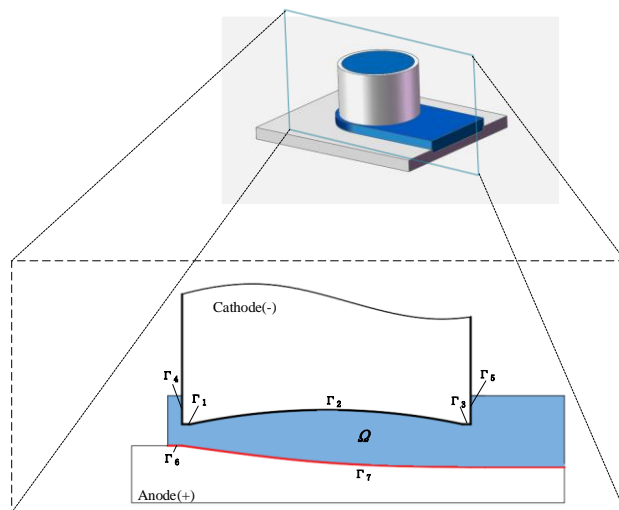


**Figure 5.** Electric field simulation model.

### 3.2 Electric field simulation conditions and result analysis

The established physical field model was imported into COMSOL Multiphysics 5.4 simulation software, and the simulation parameters are shown in Table 1.

**Table 1.** Electric field simulation parameters.

Parameter	Value
Applied voltage[V]	40
Machining gap[mm]	0.3
Electrolyte conductivity [S/m]	23.9
Feeding speed[mm/min]	60

Fig.6(a)-(d) shows the simulation results of the current density distribution in the machining area of the four tools. For tool A, the current density on the anode workpiece surface is distributed in a stepped pattern, with the highest current density near the feed direction (the smallest machining gap) and the lowest current density near the area already being machined (the largest machining gap). For tools B, C, and D, the current density distribution changed owing to the use of a circular arc surface at the bottom, which artificially increased the machining gap. Therefore, the current density in the centre area of the arc surface is significantly weakened, and the farther the distance from the centre, the less the effect. Compared with the simulation analysis of the tapered-bottom tool[15], the arc-bottom tool also reduced the current density, and this paper took into account the effect of different curved surface heights on the size of the machining gap, which changed the magnitude and distribution of the current density.

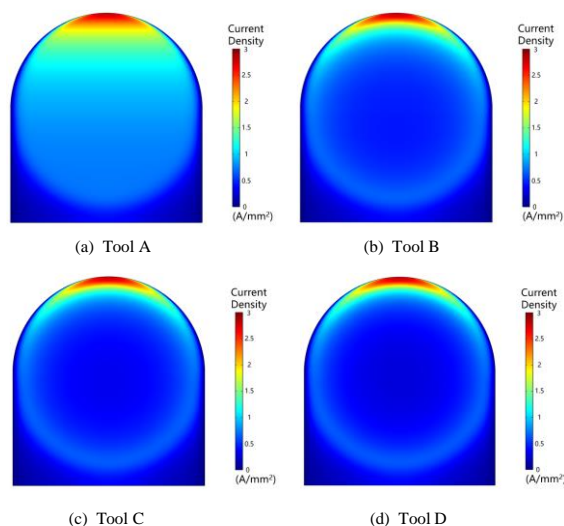


**Figure 6.** Current density distribution in the anode processing area.

Fig.7 shows the distribution of the charge passing along the bottom of the groove for the four tools, and the distribution of the charge  $Q$  at the bottom of the groove can be calculated according to the formula (7) [14]:

$$Q = \int_0^t i dt \quad (7)$$

It can be seen that the height of the arc surface at the cathode end has a significant effect on the charge distribution in the machined grooves.

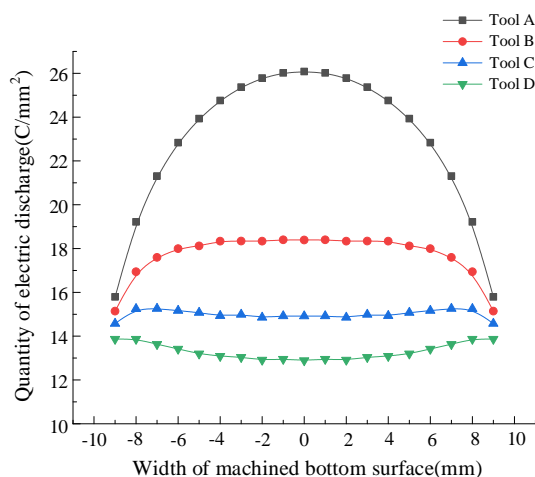


**Figure 7.** Distribution of charge along the width of the groove bottom.

For tool A, the amount of charge passing through the middle region of the machined groove is the highest, with a maximum of  $26.08 \text{ C/mm}^2$ , decreasing rapidly from the centre to the edge region. For tool B, the amount of charge passing through the centre area of the machined groove is significantly lower, with a maximum of  $18.39 \text{ C/mm}^2$ , and the variation of charge on the machined surface becomes minor from the centre to the edge area. For tool C, the amount of charge passing through the central

region of the machined groove is further reduced compared with tools A and B. Within a certain range, the charge passing through all points on the machined surface is approximately equal, with an average value of  $15.04 \text{ C/mm}^2$ . For tool D, the charge passing through the centre area of the machined groove is  $12.89 \text{ C/mm}^2$ , and the charge passing through part of the area on either side is greater than the centre area. In summary, the circular arc surface on the tool bottom reduces the current density such that a similar amount of charge passes through each part of the groove, and the most uniform amount of charge passing through the machined area is achieved when the height is 2 mm. Niu [14] Pointed out that the distribution of insulation on the bottom of the tool could change the distribution of the conductive area, which affected the distribution of charge. However, the simulation result showed that changing the height of the curved surface on the tool bottom could also affect the distribution of charge, the essence of both was to change the current density to achieve the average distribution of the charge.

## 4. EXPERIMENTAL

### 4.1 Experiment preparation and procedure

Fig.8 shows a physical photograph of four sets of tools made of stainless steel 304 with a bottom diameter of 20 mm and a height of 60 mm. The side wall was treated with electrophoresis insulation(thickness is negligible) to reduce the corrosion of the side wall electric field to the workpiece. The workpieces used for the experiments were  $\text{TiB}_2/7050$  aluminum matrix composite sheets with dimensions of  $140 \text{ mm} \times 90 \text{ mm} \times 5 \text{ mm}$ .

During the machining experiment, the EC milling machining results of the four tools were studied, including the MRR, machining groove depth, and bottom surface flatness. The machining parameters are listed in Table 2. Under the same conditions, the current efficiency of the NaCl solution was relatively high, so the MRR was high, therefore a NaCl solution with a mass fraction of 20% and a temperature of  $30 \text{ }^\circ\text{C}$  was used as the electrolyte. [24,25] Tool rotation can improve the surface quality and accuracy of machining, while a certain electrolyte pressure can renew the electrolyte in the machining gap, and increasing the cathode feed rate can improve the uniformity of the machining surface, so the electrolyte pressure was 0.3 Mpa, the spindle speed was 500 rpm, and the machining voltage, machining gap, and feed rate were the same as the simulation conditions, 40 V, 0.3 mm and 60 mm/min, respectively. [26,27] Based on these machining conditions, the simulation results were verified, and three sets of repetitions were performed to reduce the experimental error. Different initial machining gaps have the most significant influence on the flatness of the bottom surface of the machined groove. To further investigate the effect of the tools with different heights of arc surfaces in the end on the flatness of the machined groove under different initial machining gaps, four tools were tested at initial machining gaps of  $d = 0.2 \text{ mm}$  and  $d = 0.5 \text{ mm}$ , and the machining results of the four tools were compared. Finally, a sample was machined by EC milling with the optimal tool and suitable machining parameters. The machining groove profile and flatness of the bottom surface in the experimental results were measured using a wide-area three-dimensional(3D) measurement system (KEYENCE VR-5000,

Japan). The sample was ultrasonically cleaned and weighed before and after machining using an ultrasonic cleaner and high-precision electronic scale to calculate the material removal mass.



**Figure 8.** Physical photos of the tools and TiB<sub>2</sub>/7050 aluminum matrix composite workpiece

**Table 2.** Machining parameters of EC milling

Parameter	Value
Applied voltage[V]	40
Feeding speed[mm/min]	60
Spindle speed[rpm]	500
Electrolyte concentration[wt.%]	20%NaCl solution
Electrolyte pressure[Mpa]	0.3
Electrolyte temperature[°C]	30
Machining gap[mm]	0.3,0.2,0.5
Workpiece material	TiB <sub>2</sub> /7050 aluminum matrix composite

#### 4.2 Results and discussion

Four electrolyte inner-jet EC milling tools were studied for machining TiB<sub>2</sub>/7050 aluminum matrix composites at the experimental parameters shown in Table 3.

**Table 3.** Experimental parameters for EC milling

Experiment	Applied voltage[V]	Machining gap[mm]	Electrode feed rate[mm/min]	Machining length[mm]
1	40	0.3	60	55
2	40	0.2	60	55
3	40	0.5	60	55

The machining path was straight, the straight machining distance was 55 mm, and the remaining machining conditions are listed in Table 2.

4.2.1 Analysis of experimental results for machining gap  $d = 0.3$  mm

Fig.9 shows the actual machining results of the four tools at an initial machining gap of  $d = 0.3$  mm. Fig.9(a) and (b) show the top physical view and depth schematic of the machined grooves, respectively. Grooves from left to right were machined by tools A, B, C, and D in sequence. It can be observed that the depth of the grooves machined by tools A and B had a stepped distribution. From the edge of the groove to the centre, it gradually became deeper. The depths of the grooves machined by tools C and D were significantly shallower than that of tool A. With an increase in the arc surface height, the groove depth became increasingly shallower. However, the depth of the grooves was more consistent, that was, the bottom surface had a better flatness. Fig.9(c) shows the profile of the machining groove obtained by measuring along the blue line in Fig.9(a), from which it can be seen that the depth of the profile of the machining groove of tools A-D became shallower in order. The deepest depths of the grooves were -0.834 mm, -0.609 mm, -0.509 mm, and -0.446 mm, respectively. The groove machined by tool A was a concave U-shaped groove, the groove machined by tool B was improved, but was still concave, the groove machined by tool D had a clear upward convex feature in the centre area, and the groove machined by tool C was the flattest. Therefore, from the groove profile diagram, the flatness of the bottom surface of the groove machined by tool C with the centre height of the arc surface at the end of the tool being 2mm was the best, which was consistent with the simulation analysis results. This demonstrated that the curved surface tool could vary the magnitude of the current density so that the distribution of the charge in the processing area was more uniform, and the groove bottom surface was flatter than that of the flat tool.

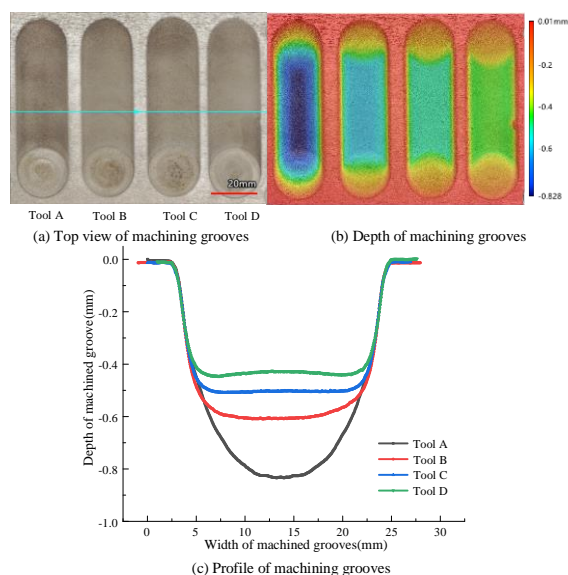
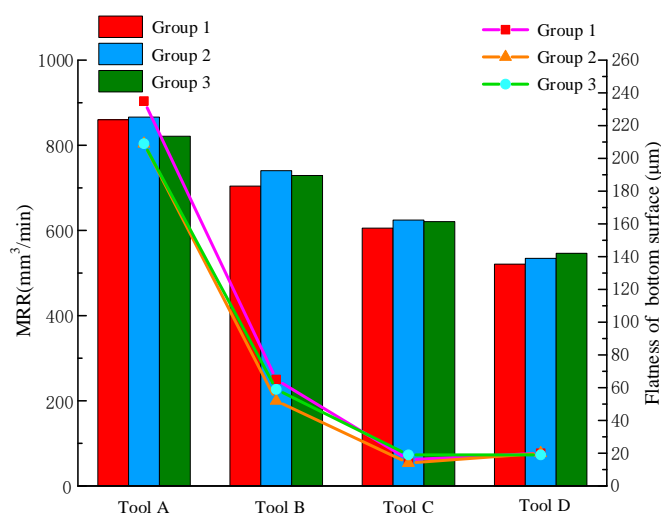


Figure 9. Grooves machined by four tools for a machining gap of  $d = 0.3$  mm

The three replicate experiments of Groups 1-3 in Fig.10 show the MRR and groove bottom flatness of the machined TiB<sub>2</sub>/7050 aluminum matrix composite workpiece for four tools with an initial machining gap of  $d = 0.3$  mm. Fig.10 shows that the MRR of the workpiece emerged a decreasing trend as the height of the arc of the tool end increased, and the MRR of the grooves machined by tools A-D in Group 1 (Fig.9) were 788.429 mm<sup>3</sup>/min, 645.434 mm<sup>3</sup>/min, 555.174 mm<sup>3</sup>/min, and 477.534 mm<sup>3</sup>/min, respectively. The reason for the decrease in the MRR was that the machining gap in the machining area of tools A-D gradually increased, and the current density in the machining area declined. Therefore, the amount of charge passing through descended, and the depth of the grooves and MRR decreased. The MRR of tool C decreased by 29.58% compared to tool A, and the other two groups decreased by 27.91% and 24.41%, respectively. The flatness of the groove bottom surface indicates the difference between the highest and lowest points in the cross-sectional range of the groove bottom surface. The smaller the difference, the higher the flatness. The bottom surface flatness of the grooves machined by tools A-D in Group 1 was 235 μm, 65 μm, 13 μm, and 20 μm, respectively; the bottom surface flatness of tool C was 94.47% higher than that of tool A, and the other two groups were 93.30% and 90.91%, respectively. The reason for the upward convex feature of the bottom surface machined by tool D compared with tool C was that the amount of charge passing through the centre region of the machined groove during tool machining was smaller than the amount of charge passing through the sides, that was, the MRR in the centre region of the machined groove was smaller than that on both sides of the centre of the groove, which resulted in an upward convexity at the bottom of the groove. In summary, a tool with an arc surface end can improve the flatness of the bottom surface of the machined groove, but at the expense of reducing MRR. In the case where the machining gap  $d = 0.3$  mm, the bottom surface flatness of the groove machined by tool C with a tool end arc surface height of 2 mm was the best, followed by tool D and B, and that for tool A was worse.



**Figure 10.** MRR and bottom flatness of four tools for a machining gap of  $d = 0.3$  mm

4.2.2 Analysis of the experimental results for machining gap  $d = 0.2$  mm

Fig.11 shows the actual machining results of the four tools at an initial machining gap of  $d = 0.2$  mm. Similar to Section 4.2.1, in Fig.11(a) and (b), the depths of the grooves machined by tools A and B had a clear step-like distribution, and the depths of the grooves machined by tools C and D were smaller than those of tool A, but the bottom surface had better flatness; in Fig.11(c), the deepest depths of the grooves machined by tools A-D were: -0.914 mm, -0.692 mm, -0.579 mm and -0.487 mm. The grooves machined by tools A and B were still concave, and the grooves machined by tools C and D had an upward convex feature in the centre region, but the bottom surface of the grooves machined by tool C was flatter than that of tool D. The reason for the upward convexity was that the height of the arc surface of the tool end was too high when the machining gap  $d = 0.2$  mm, causing the amount of charge passing through the centre region of the groove to be less than that on the two sides, and the MRR in the centre region to be less than that on the two sides. A flatter groove bottom surface may be machined by a tool with an end arc height between 1mm and 2mm.

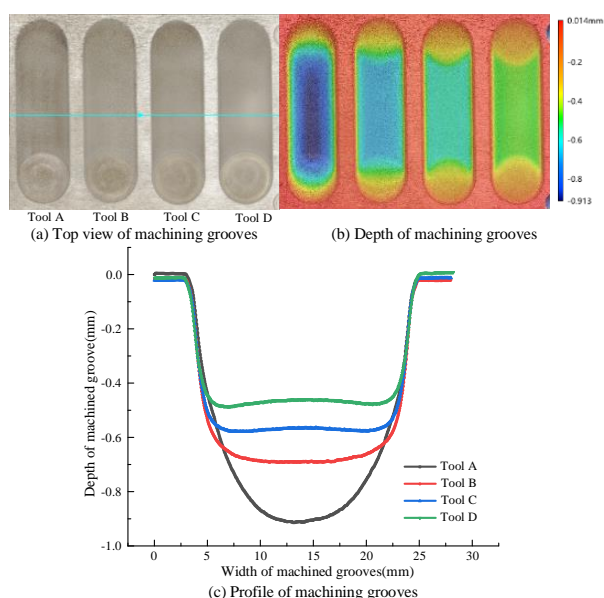


**Figure 11.** Grooves machined by four tools for a machining gap of  $d = 0.2$  mm.

The three replicate experiments of Groups 1-3 in Fig.12 represent the MRR and groove bottom flatness of the TiB<sub>2</sub>/7050 aluminum matrix composite workpiece machined using the four tools at an initial machining gap of  $d = 0.2$  mm. As the height of the tool end arc surface increased, the MRR still appeared a decreasing trend, However, the decrease of the initial machining gap increased the corresponding MRR compared to the machining gap of  $d=0.3$ mm and the reason was that the current density and the amount of charge increased which enhanced the MRR. The MRR for tools A-D in Group 1 (Fig.11) were 852.731 mm<sup>3</sup>/min, 742.498 mm<sup>3</sup>/min, 631.963 mm<sup>3</sup>/min, and 522.781 mm<sup>3</sup>/min, respectively, with a 25.89% decrease in MRR for tool C compared to tool A, and the other two groups decreased by 27.78% and 26.19%, respectively. The bottom flatness of tools A-D was 228 μm, 52 μm, 16 μm, and 27 μm, respectively, and tool C was better than tool D. For tool C, the bottom flatness was

improved by 92.98% compared with tool A, and the other two groups were improved by 93.01% and 93.30%, respectively. Therefore, in the case where the machining gap  $d = 0.2$  mm, the bottom surface flatness of the groove machined by tool C with the tool end arc surface height of 2 mm was still the best and the reason was the charge through the processed area was more uniform, followed by tool D and B, and that for tool A was worse.

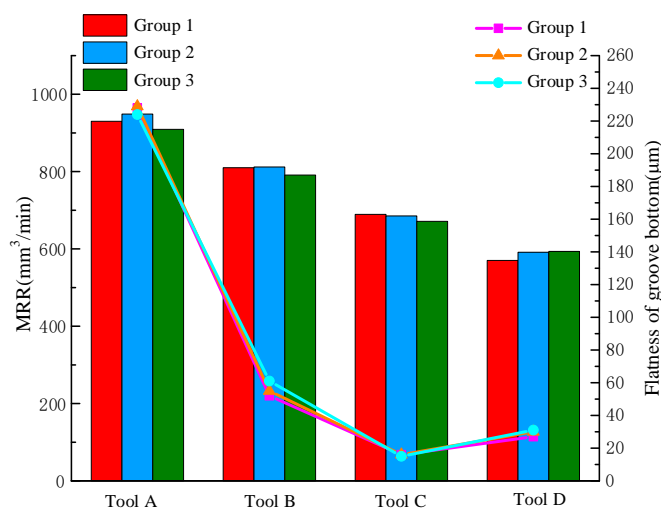


**Figure 12.** MRR and bottom flatness of four tools for a machining gap of  $d = 0.2$  mm.

#### 4.2.3 Analysis of experimental results when machining gap $d = 0.5$ mm

Fig.13 shows the machining results of the four tools under the initial machining gap of  $d = 0.5$  mm. In Fig.13(a) and (b), it can be seen that the depths of the grooves machined by tools A and B still had a precise stepped distribution, and the depths of the grooves machined by tools C and D were shallower, but the flatness of the bottom surface was better than that of the other tools. The deepest depths of the grooves machined by tools A-D in Fig.13(c) were  $-0.680$  mm,  $-0.517$  mm,  $-0.438$  mm, and  $-0.379$  mm, respectively.

Compared with the machining gap of  $d = 0.3$  mm, the depths of grooves were reduced, the reason was that the increase in the machining gap decreased the current density and the amount of charge passing through, which in turn reduced the machining depth. The grooves machined by tools A and B were still concave, while the groove machined by tool C also had a concave feature, and the bottom surface of the groove machined by tool D was flatter because its arc surface provided a more uniform distribution of charge in the machining area.

The three repeated experiments of Groups 1-3 in Fig.14 represent the MRR and groove bottom surface flatness of the four types of tools under the initial machining gap of  $d = 0.5$  mm. The MRR of tools A-D in Group 1 (Fig.13) were  $668.306$  mm<sup>3</sup>/min,  $596.153$  mm<sup>3</sup>/min,  $517.214$  mm<sup>3</sup>/min, and  $451.805$  mm<sup>3</sup>/min, respectively, and the MRR of tools C and D respectively decreased by 22.61% and 32.40% compared to tool A. The bottom surface flatness machined by tools A-D were  $212$  µm,  $57$  µm,  $19$  µm, and  $6$  µm, respectively, and the bottom surface flatness of tools C and D was respectively

improved by 91.04% and 97.17% compared to tool A. Compared with the machining gaps of  $d = 0.3$  mm and  $d = 0.2$  mm, in the case where the machining gap  $d = 0.5$  mm, the bottom surface of the groove machined by tool D with the tool end arc height of 3 mm was the best, tool C and B were next, and that for tool A was worse. The possible reason was that when the initial gap increased, the amount of charge passing through the central machining area of tool C was slightly smaller than that of the two sides, while the distribution of charge in the machining area corresponding to tool D was more uniform.

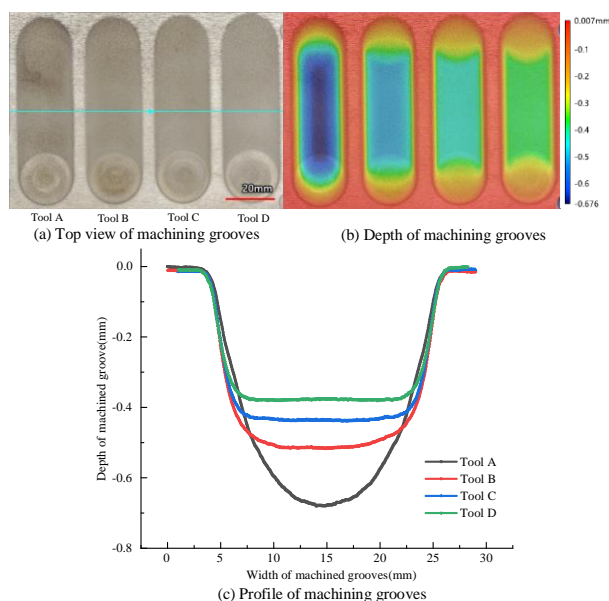


Figure 13. Grooves machined by four tools for a machining gap of  $d = 0.5$  mm.

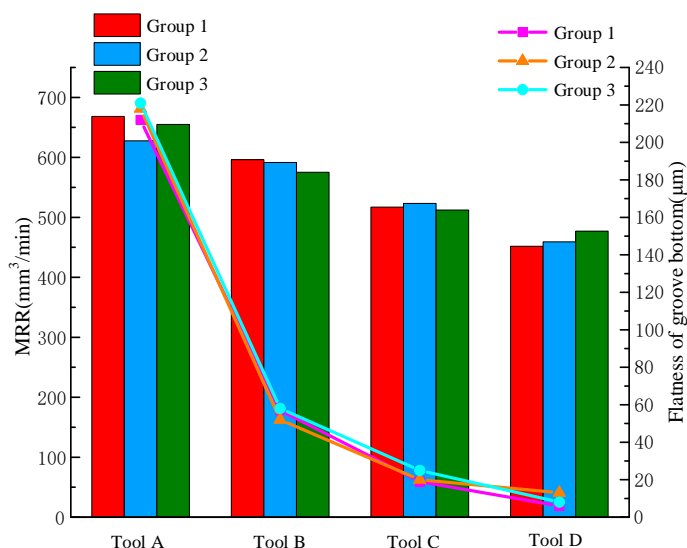
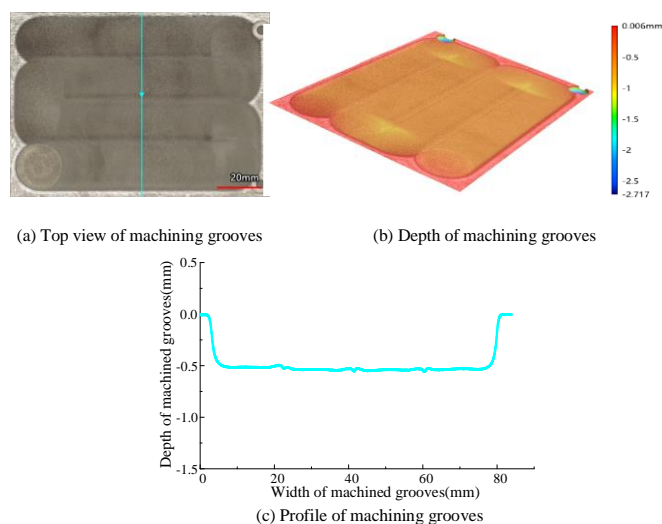


Figure 14. MRR and bottom flatness of four tools for a machining gap of  $d = 0.5$  mm

For embedded EC milling, Niu[14] improved the groove bottom flatness by about 58% with a bottom insulating tool and a higher machining voltage, Li[15] greatly enhanced the groove bottom flatness with a tapered bottom tool but found that the groove bottom flatness would be decreased with much higher voltage, and Yue[28] improved the flow field of the machining gap by using a bottom open-

hole tool which enhanced the groove bottom flatness about 30%. This paper investigated EC milling of TiB<sub>2</sub>/7050 aluminum matrix composite workpiece, and the flatness of machined groove bottoms was increased by more than 90% with different arc surface heights of tool bottoms and initial machining gaps, which was a complement to the method of EC milling of groove and improvement of groove bottom flatness.

With an initial machining gap of  $d = 0.3$  mm or  $d = 0.2$  mm, a flatter groove on the bottom surface can be machined by tool C compared with other tools. A sample of TiB<sub>2</sub>/7050 aluminum matrix composite workpiece was machined using tool C. As shown in Fig.15, the machining voltage  $U = 40$  V, the machining gap  $d = 0.3$  mm, the feed rate  $V_f = 60$  mm/min, four consecutive round trips, each machining distance of 90 mm, traverse amount of 19 mm, and the rest of the machining conditions were listed in Table 2. Fig.15(a) and (b) provided the top physical view and depth schematic of the groove machined by tool C. The entire machining area was approximately 110-mm long and 80-mm wide, and the depth of the machining area tended to be consistent. Fig.15(c) demonstrated the profile of the machined groove measured by the blue line in Fig.17(a), and the machined depth was 0.51mm. The total mass removed by the machining was 11.6g, the average flatness of the groove was 18  $\mu$ m, and the surface roughness of the groove was 11.292 $\mu$ m.



**Figure 15.** Plane for EC milling of tool C.

## 5. CONCLUSION

This paper proposes three tools with different tool end arc surface heights for EC milling and compares them using a flat-bottom tool. By performing electric field simulations and experimental studies using four tools, the following conclusions can be summarized as follows:

(1) The electric field simulation shows that setting the tool end with a concave arc surface can reduce the current density. The higher the centre of the arc surface, the lower will be the current density, and the arc tool can distribute the amount of charge passing through the machining area to be more

uniformly. The electricity passing through the machining area was most even when the machining gap was 0.3 mm, and the height of the centre of the arc surface at the end of the tool was 2 mm;

(2) The experimental results indicate that in the process of EC milling of TiB<sub>2</sub>/7050 aluminum matrix composites, a tool with an arc surface at the end can improve the bottom surface flatness of the machined groove; however, this was at the expense of reducing the MRR. When the machining gap  $d = 0.3$  mm, the bottom surface flatness of the groove machined by tool C with the tool end arc surface height of 2 mm was the best, which was 13  $\mu\text{m}$ . Compared with the flat-bottom tool, the flatness of the bottom surface was increased by 94.47%, but the corresponding MRR was reduced by 29.58%.

(3) Experiments comparing different machining gaps show that for a machining gap of  $d = 0.2$  mm, the bottom surface of the groove machined by tool C with the centre height of the arc surface at the tool end of 2 mm had the best flatness of 16  $\mu\text{m}$ ; for a machining gap of  $d = 0.5$  mm, the bottom surface of the groove machined by tool D with the centre height of the arc surface at the tool end of 3 mm had the best flatness of 6  $\mu\text{m}$ .

#### ACKNOWLEDGEMENTS

This research is supported by the National Natural Science Foundation of China (Grant No. 51875286) and the National Natural Science Foundation of China for Creative Research Groups (Grant No. 51921003).

#### References

1. Y. Ma, Z. Chen, M.L. Wang, D. Chen, N.H. Ma, H.W. Wang, *Mater. Sci. Eng., A*, 640 (2015) 350–356.
2. M. Wang, Y. Wang, J. Liu, Z. Chen, H. Chen, Y. Wu, F.G. Zhang, H.W. Wang, *Mater. Sci. Eng., A*, 742 (2019) 364–372.
3. H.H. Sun, Y.B. Ren, Y. Feng, H.Q. Ba, D. Chen, C.J. Xia, H.W. Wang, *Def. Technol.*, 17 (2021) 1062–1070.
4. K.Y. Lin, W.H. Wang, R.S. Jiang, Y.F. Xiong, D.Z. Zhao, *Materials*, 11 (2018) 706.
5. Q. Gao, S.S. Wu, S.L. Lu, X.C. Duan, P. An, *Mater Des*, 94 (2016) 79–86.
6. K.Y. Lin, W.H. Wang, R.S. Jiang, Y.F. Xiong, *Int. J. Adv. Manuf. Technol.*, 100 (2019) 143–151.
7. Y.F. Xiong, W.H. Wang, R.S. Jiang, K.Y. Lin, G.D. Song, *Int. J. Adv. Manuf. Technol.*, 86 (2016) 3517–3526.
8. K. Mishra, B.R. Sarkar, B. Bhattacharyya, *Mater. Manuf. Processes*, 34 (2019) 807–813.
9. S. Hinduja, J. Pattavanitch, *CIRP J Manuf Sci Technol*, 12 (2016) 79–89.
10. M.M. Lohrengel, K.P. Rataj, T. Munninghoff, *Electrochim. Acta*, 201 (2016) 348–353.
11. J.Z. Zhang, Z.H. Shen, N.S. Qu, *Int. J. Adv. Manuf. Technol.*, 121 (2022) 7933–7948.
12. Z.S. Ye, G.L. Qiu, X.L. Chen, *Micromachines (Basel)*, 13 (2022) 1051.
13. B.S. He, H.S. Li, X. Ma, J. Li, S.K. Fan, *Appl. Sci.-Basel*, 11 (2021) 8087.
14. S. Niu, N.S. Qu, H.S. Li, *Int. J. Adv. Manuf. Technol.*, 97 (2018) 1371–1382.
15. H.S. Li, S.X. Fu, Q.L. Zhang, S. Niu, N.S. Qiu, *Chin. J. Aeronaut.*, 31 (2018) 608–616.
16. S. Skoczypiec, P. Lipiec, W. Bizoń, D. Wszyński, *Materials*, 14 (2021) 2248.
17. W.D. Liu, S.S. Ao, Y. Li, Z.M. Liu, H. Zhang, S.M. Manladan, Z. Luo, Z.P. Wang, *Electrochim. Acta*, 233 (2017) 190–200.

18. C.Y. Zhang, J.L. Yao, C.Y. Zhang, X.L. Chen, J.W. Liu, Y.J. Zhang, *J Mater Process Technol*, 282 (2020) 116695.
19. K. Mishra, B.R. Sarkar, B. Bhattacharyya, *Mach. Sci. Technol.*, 26 (2022) 18–48.
20. H.S. Li, S. Niu, Q.L. Zhang, S.X. Fu, N.S. Qu, *Sci Rep*, 7 (2017) 1–11.
21. X.M. Zhang, X.D. Song, P.M. Ming, X.C. Li, Y.B. Zeng, J.T. Cai, *Micromachines (Basel)*, 10 (2019) 404.
22. D. Zhu, K. Wang, J.M. Yang, *CIRP Annals*, 52 (2003) 169–172.
23. W.D. Liu, Z. Luo, Y. Li, Z.M. Liu, K.B. Li, J.X. Xu, S.S. Ao, *Int. J. Adv. Manuf. Technol.*, 100 (2019) 2357–2370.
24. H. Wang, J. Liu, D.W. Gu, D. Zhu, *Int. J. Electrochem. Sci.*, 15 (2020) 9313–9324.
25. L. Tang, B. Li, S. Yang, Q.L. Duan, B.Y. Kang, *Int. J. Adv. Manuf. Technol.*, 71 (2014) 1825–1833.
26. X.D. Wang, N.S. Qu, X.L. Fang, H.S. Li, *J Mater Process Technol*, 238 (2016) 1–7.
27. K. Mishra, S. Sinha, B.R. Sarkar, B. Bhattacharyya, *Advances in Unconventional Machining and Composites*, Springer, (2020), pp. 527–535.
28. X.K. Yue, N.S. Qu, S. Niu, H.S. Li, *J Mater Process Technol*, 276 (2020) 116413.

© 2022 The Authors. Published by ESG ([www.electrochemsci.org](http://www.electrochemsci.org)). This article is an open access article distributed under the terms and conditions of the Creative Commons Attribution license (<http://creativecommons.org/licenses/by/4.0/>).